Comparison of the axial resolution of practical Nipkow-disk confocal fluorescence microscopy with that of multifocal multiphoton microscopy: theory and experiment

A. EGNER, V. ANDRESEN & S. W. HELL
High Resolution Optical Microscopy Group, Max-Planck-Institute for Biophysical Chemistry,
Göttingen, Germany

Summary

We compare the axial sectioning capability of multifocal confocal and multifocal multiphoton microscopy in theory and in experiment, with particular emphasis on the background arising from the cross-talk between adjacent imaging channels. We demonstrate that a time-multiplexed non-linear excitation microscope exhibits significantly less background and therefore a superior axial resolution as compared to a multifocal single-photon confocal system. The background becomes irrelevant for thin (< 15 μm) and sparse fluorescent samples, in which case the confocal parallelized system exhibits similar or slightly better sectioning behaviour due to its shorter excitation wavelength. Theoretical and experimental axial responses of practically implemented microscopes are given.

Introduction

In parallelized confocal (Petran *et al.*, 1968; Kino & Corle, 1989) and non-linear scanning fluorescence (Bewersdorf *et al.*, 1998; Buist *et al.*, 1998) microscopy, scanning is accomplished with an array of foci rather than with a single beam. As a result, the image acquisition time is cut down by the number of foci applied. Major advantages of parallelization are that real-time imaging is achieved (Bewersdorf *et al.*, 1998) and images of weakly fluorescent objects are recorded within a much shorter time (Straub *et al.*, 2000). Perhaps the only drawback of parallelization is that for a high density of foci, the axial sectioning of the system is degraded by cross-talk between the foci (Sheppard & Wilson, 1981; McCabe *et al.*, 1996; Buist *et al.*, 1998; Egner & Hell, 2000). Therefore a significant part of the early literature on parallelized (Nipkow-type) confocal 3D-imaging concentrated on the trade-off between optical axial sectioning and parallelization.

Correspondence to: S. W. Hell. Fax: +49 551 201 1085; e-mail: hell@4pi.de

An elegant approach to this problem is aperture correlation microscopy (Juškaitis *et al.*, 1996). In this microscope the foci are densely and randomly arranged, so that the strong cross-talk arising in the recorded image adds up to a conventional image. The confocal image is readily gained by recording a conventional image separately and by subtracting this image from that of the correlation microscope. The limitation of this concept is that mathematical subtraction fails in the presence of noise, which is particularly relevant if the conventional image is very bright with respect to the confocal image to be gained.

Lately however, an all-optical remedy for background has been found, which is time-multiplexing (TMX) in conjunction with non-linear pulsed microscopy. TMX means that interference between neighbouring excitation fields is precluded by ensuring that the pulses in each of the foci pass through the sample at different time-points (Buist *et al.*, 1998; Egner & Hell, 2000; Fittinghoff *et al.*, 2000; Nielsen *et al.*, 2001). The ability of TMX to provide much crisper 3D-images has been demonstrated recently with a TMX scheme producing three non-interfering subgroups of foci in a multifocal multiphoton microscope (MMM) (Andresen *et al.*, 2001). We refer to it here as TMX-3, with the number 3 referring to the three subgroups. Although it is applicable only in non-linear imaging, TMX-mode non-linear microscopy is important because it constitutes the first solution to this classical conflict between sectioning and parallelization in 3D-imaging. In a TMX-*N* non-linear microscope with *N* foci, all the foci are time-multiplexed, so that it allows for non-compromised parallelization even for interfocal distances smaller than the wavelength. The foci can be made to overlap so that focal plane scanning could be made obsolete.
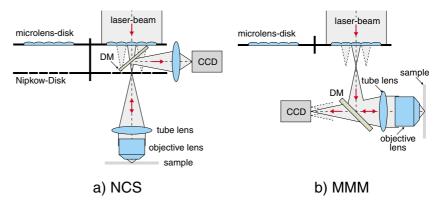
The recent success of these systems at high resolution 3D-imaging motivated us to compare the axial sectioning of a (time-multiplexed) parallelized non-linear microscope with that of a parallelized single-photon confocal fluorescence

Fig. 1. Nipkow confocal scanner (NCS) and multifocal multiphoton microscope (MMM): (a) in the NCS an array of pinholes on a rotating disk splits the laser beam into beamlets, producing an array of diffraction-limited foci in the sample. The fluorescence is imaged through the pinholes onto a CCD-camera; for this purpose the dichroic mirror has to be placed between the pinhole array and the microlenses. The microlenses augment the throughput of the laser light but are not critical for image formation. (b) In the MMM an array of microlenses on a rotating disk splits the beam of a mode-locked laser into beamlets, producing an array of diffraction limited foci in the sample. The fluorescence signal is imaged onto a CCD-camera.

scanner. We investigated the UltraVIEW LCI Confocal Optical Scanner by Perkin-Elmer Life Sciences (Cambridge, UK) as a representative of the latter, which we refer to here as the Nipkow confocal scanner (NCS) (Ichihara *et al.*, 1996). In this paper we analyse its imaging capabilities theoretically and experimentally, and compare it directly with the multifocal multiphoton microscopy and TMX-3-MMM developed in our laboratory (Egner & Hell, 2000; Andresen *et al.*, 2001). For our theoretical analysis we have chosen conditions that are as close as possible to those in the practical systems. Conclusions are drawn that are valid for further improving parallelization in 3D-microscopy.

Microscopes

A common feature of our parallelized 3D-microscopes is that both rely on the Nipkow-spiral arrangement for scanning. The spiral arrangement is probably the most convenient way of parallelizing 3D-microscopy. It is attractive not only because of its simplicity and ruggedness, but also because it does not involve scanning dead times, as is often the case in galvanometric scanning. Not surprisingly, Nipkow-type scanning has been accomplished both in early confocal microscopes, but also in the earliest form of MMM (Fig. 1). We note, however, that the Nipkow-type scanning is irrelevant for their sectioning ability.

Another common feature is that in all systems the laser first impinges on microlenses that are arranged on a fused silica disk in the Nipkow-type fashion (Ichihara *et al.*, 1996). Again, one should not be distracted by this common optical element, because the physical role of the microlenses is different in each case. Being a single-photon excitation confocal microscope, the NCS uses a pinhole array disk (Fig. 1). The pinholes are arranged in the Nipkow-type fashion and serve both for illumination and detection in the confocal setting. The microlens disk is adapted to the Nipkow-disk and its role is to focus the laser beams into the pinhole array, so that only little laser light is wasted or reflected from the back side of the disk. Therefore, a smaller and less bulky laser can be employed. The microlenses do not increase the irradiance or brightness of the laser,

of course, because the irradiance is a property of the laser itself that cannot be changed by passive optical elements. Evidently, the microlenses also have no influence on the collection of the fluorescence light. The real advantage of the microlenses is that the level of stray laser light hitting the back side of the disk is strongly reduced. The fluorescence throughput and the resolution are determined entirely by the size of the pinholes and the density of the foci in the sample. In principle, in the NCS the microlens array could be removed without eliminating its sectioning and scanning abilities. Moreover, the microlenses are not an integral part of the image formation or the sectioning procedure. By contrast, the microlens array or a similar beam splitting device is essential in the MMM. If removed, 3D-imaging would not be possible.

TMX-3-MMM is accomplished by a holey mask with different glass thickness firmly attached to the microlens disk (Egner & Hell, 2000; Andresen *et al.*, 2001). The difference in optical path lengths ensures that neighbouring pulses require additional time required to pass through the glass mask. In our case this is typically of the order of 0.5 ps. Finally, we note that MMM uses a rather complex, mode-locked Ti:sapphire laser emitting pulses of 200 fs duration at a repetition rate of 76 MHz, whereas NCS employs a standard continuous wave argon-krypton laser oscillating on several lines. In both systems, the fluorescence is imaged onto a CCD-camera. Whereas in the NCS the fluorescence has to be spatially filtered by the array of pinholes, in the MMM the fluorescence is directly imaged onto the CCD-camera as in a conventional microscope.

Theory and parameters of calculations

First, we compare the two systems in terms of their z-response, which is the axial response to an infinitely thin fluorescent layer. The z-response is a good measure for the sectioning ability of the microscopes. For two-photon excitation, the z-response of the TMX-N-MMM is given by:

$$I_{z,MMM}(z) = \sum_N \iint |h \otimes g^N_{MMM}|^4 \, dxdy \qquad (1)$$

h is the amplitude PSF of the objective lens, that is the field generated by a single beamlet in its focal region. It is convoluted with the grating function g_{MMM}^N describing the coordinates of the array. The convolution automatically takes into account the interferences between the focal fields. The index N and the summation stem from the fact that we have to add the responses of the N subgroups incoherently.

The z-response of the NCS has to take into account the imaging of the illuminated pinholes of the Nipkow-disk into the focal plane and the back-imaging of the resulting fluorescence onto the pinholes described by the function $p = p(x, y)$ $= 1$ for $\sqrt{x^2 + y^2} \leq p_0$, with p_0 being the radius of the detection pinholes projected into the focal plane. Therefore, the response of the NCS is given by:

$$I_{z,NCS}(z) = \iint |h_{\lambda-exc} \otimes g_{NCS}|^2 \cdot ((|h_{\lambda-det}|^2 \otimes p) \otimes g_{NCS}) dx dy \quad (2)$$

The effective PSF of the system is obtained by multiplying the excitation part with the detection part, which is also obtained by convolving the detection PSF, calculated at the fluorescence wavelength, with the grating function g_{NCS} containing the location and the size of the pinholes in the Nipkow-disk. For the illumination, the size of the pinholes can be largely ignored, not only because the laser light is coherent, but also because the waist of the foci produced by the microlenses is smaller than the pinholes and the associated back-projected Airy disk of high aperture lenses.

Another useful measure of the sectioning strength of a 3D-microscope is the sea response:

$$I_{sea}(z) = \int_{\infty}^2 I_z(z') \, dz', \quad (3)$$

which is the integral of the z-response and describes the signal generated by a fluorescent half-space that is moved along the optic axis. Although it does not contain new physical information with respect to the z-response, it highlights the ability of the system to discriminate a small or faint object above or beneath a bright, extended one – the most extreme case in optical sectioning.

For our calculations we have chosen parameters that are as close as possible to the realized optical microscopes, because we were interested in explaining the behaviour of the currently available systems. We have elected an effective NA = 1.35 (oil immersion, $n = 1.518$), which is typical for high-resolution optical microscopy. Furthermore, we considered a hexagonal arrangement of 37 foci in the focal plane, which corresponds to the MMM set-up we have built in our laboratory. The number is determined by the total power that is emitted from our Ti:sapphire oscillator (1.5 W), as we have to ensure that, after all losses in the system, 10 mW of time-averaged power arrive in each focus. Requiring much less laser power, the single-photon excitation-based NCS illuminates the sample with as many as 1000 foci. Although at a given interfocal distance it allows for a larger field of view, such a high number of foci degrades the sectioning ability of the system, simply because there are more confocal channels that cross-talk with each other. The calculation of the PSF and the evaluation of the equations are performed numerically.

In order to first reveal the causes of differences between the two systems that are more related to the imaging mode, we have decided to consider 37 foci in the NCS as well. The consideration of N = 1000 is computationally more extensive because it requires the exact calculation of the very high order three-dimensional structure of the side maxima. The smaller number of foci makes the z- and sea-responses of NCS look better in the calculation than in reality. The reason is that fewer foci are associated with less cross-talk. Another reason for considering fewer confocal channels is that a laterally extended object extending over the whole field of view occurs rather rarely. In addition, it makes sense to compare the sectioning strength of objects of similar lateral extent. Still, we will also vary the total number of foci to give a feel for the effect of the field of view.

Clearly the ratio between the interfocal distances and the wavelengths, and the pinhole diameter in the NCS decide about the sectioning ability of the microscopes. We have chosen not to vary the wavelength and the interfocal distances, but to settle on those parameters that are present in the practically realized microscopes. Therefore, the excitation wavelengths were elected to $\lambda_{exc,NCS} = 488$ nm and $\lambda_{exc,MMM} = 800$ nm for the NCS and the MMM, respectively. We chose $\lambda_{fluo} = 512$ nm as the fluorescence wavelength for both systems. The pinhole diameter in the Nipkow-disk of the NCS was set to the original 50 μm, and the distance between two adjacent pinholes amounts to 250 μm in this system. The use of a 100× magnification objective lens in combination with a 1.0× tube lens leads to a distance between closest neighbours in the focal plane of 2.5 μm. The pitch between two microlenses on a MMM-microlens-disk typically amounts to 400 μm, resulting in an interfocal distance of 4 μm. In order to elucidate the effect of parallelization on the sectioning, we also calculated the single-beam confocal and two-photon fluorescence responses.

Theoretical results

In Figs 2–4 we compare the three systems on the basis of our calculations. Figure 2 compares the calculated z-responses for a single-beam confocal, a single-beam two-photon microscope, the regular MMM, the TMX-3-MMM, TMX-N-MMM, as well as the NCS with the 50 μm pinholes. To emphasize the background, the responses are shown on a semi-logarithmic scale in the main panel. To give a better feel for the real dimensions, the inserted demagnified image shows the data on a linear representation. The latter shows that the responses have a similar axial full width at half maximum (FWHM) of 600–700 nm; however, there is a pronounced difference in the background signal, as can be inferred from the semi-logarithmic plot.
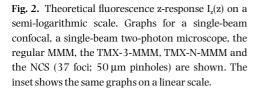
Fig. 2. Theoretical fluorescence z-response $I_z(z)$ on a semi-logarithmic scale. Graphs for a single-beam confocal, a single-beam two-photon microscope, the regular MMM, the TMX-3-MMM, TMX-N-MMM and the NCS (37 foci; 50 μm pinholes) are shown. The inset shows the same graphs on a linear scale.
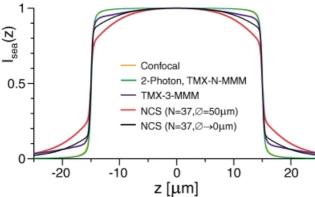

Fig. 3. Theoretical fluorescence sea-response $I_{sea}(z)$. Graphs for a single-beam confocal, a single-beam two-photon microscope, the TMX-3-MMM, TMX-N-MMM and the NCS (50 μm and 0 μm pinholes) are shown.

Fig. 4. Theoretical fluorescence z-response $I_z(z)$ of the NCS for different pinhole sizes and degrees of parallelization. To highlight the differences a semi-logarithmic scale is used.

If we leave aside the potential scattering of the fluorescence light upon imaging onto a CCD-camera, a feature typical for any conventional microscope, owing to its decoupled foci, the TMX-N-MMM behaves like an ideal single-beam scanning microscope. By contrast, the responses of the MMM and the NCS do not fall off that sharply and exhibit noticeable contributions from out-of-focal-plane regions. When imaging thin objects this 'background' may be largely neglected in all systems, but plays a role when imaging small objects that are axially adjacent to bright and bulky ones. This becomes obvious when comparing the curves in Fig. 3 displaying the calculated sea-responses for a 30 μm fluorescent sea. Clearly, the two-photon z-response of the TMX-N-MMM is identical with that of a single beam two-photon microscope, which does not have any background by definition.
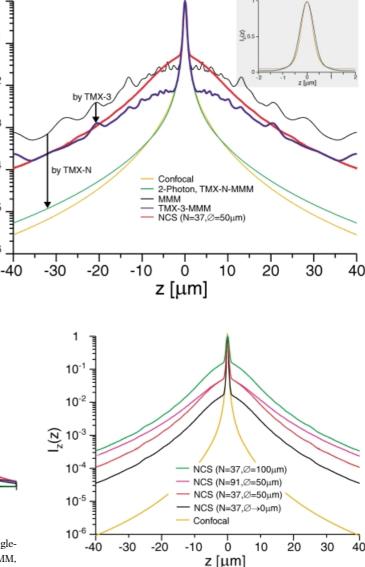
The calculations of Fig. 2 also disclose that the implementation of TMX-3, i.e. of only three time-delayed subgroups, reduces the background by about an order of magnitude, which is a substantial improvement. The superiority of the TMX-3-MMM is also witnessed in the sea-response displayed in Fig. 3. Such a mechanism does not exist in the NCS, so that it becomes obvious that the axial sectioning of a TMX-($N > 1$)-MMM, is superior to that of a parallelized confocal scanner. The semi-logarithmic plot further indicates that in the (important) region close to the focal plane the 'background' is lower in the standard MMM than in the NCS, whereas in the more remote regions ($|z| > 5$ μm), that of the NCS is slightly lower than in the standard MMM.

The apparently lower background of the NCS in the (unimportant) remote parts is due to the fact that only $N = 37$ beamlets were considered for the NCS in the calculation instead of the $N = 1000$ beamlets used in the real system, which is computationally extensive. However, we were able to cope with $N = 91$, so that Fig. 4 displays the z-responses of the NCS both for $N = 37$ (red continuous line) and for $N = 91$ (red dashed line). The comparison confirms that for $N = 91$ the remote part of the background becomes larger with an increasing number of pinholes. Both were calculated for a pinhole diameter of 50 μm, corresponding to an Airy disk, as specified by the manufacturer.

Clearly, the pinhole diameter has a strong influence on the background, as shown in Fig. 4. Even for point-like pinholes a significant background is found, stemming from the crosstalk between the N confocal channels. This background is obviously a function of the pinhole density, aperture and wavelength and should not be treated further here. Figure 4 reveals that for the 50 μm diameter pinholes and $N = 37$, an increase of the background by a factor of three takes place. By further increasing the diameter to 100 μm, the background is further raised by the same factor. Importantly, the presence of background for point-like pinholes makes evident that a NCS can never match the axial sectioning ability of a single beam confocal microscope and of a TMX-N-MMM, even under ideal circumstances.

The behaviour of the z-response can be explained intuitively as follows. If the infinitely thin plane is within the region of the main focal maximum, that is $|z| < 0.5$ μm, hardly any cross-talk occurs and each illumination pinhole creates fluorescence at the sample that is primarily back-imaged onto the same pinhole. Hence, the inner part of the z-response of the parallelized system is identical with that of a single beam microscope. For slightly larger $|z|$, cross-talk between neighbouring confocal channels occurs, in which case the diameter of the pinhole plays an important role, whereas the degree of parallelization N is of secondary importance. For strong defocus, however, almost every point of the focal plane is illuminated by each illumination channel and vice versa, so that each detection channel detects fluorescence generated by almost any other illumination channel. So in the limiting case of large $|z|$, the residual background is governed by the ratio of the area of the pinholes with respect to that of the field of view.

It becomes clear that in the NCS, the selection of an adequate pinhole diameter is critical. A reduction of the pinhole diameter to about 25 μm, that is 0.5 Airy disks, is clearly advisable. We also note that in parallelized single-photon excitation confocal microscopy, a pulsed, time-multiplexed excitation does not help to eliminate the background in the z-response. Whereas the interference between the individual illumination fields taking place in the foci is eliminated by TMX, the decisive cross-talk between the different confocal channels is not suppressed. This reasoning is confirmed by the calculation shown in Fig. 4. If an NCS could afford 'point-like'
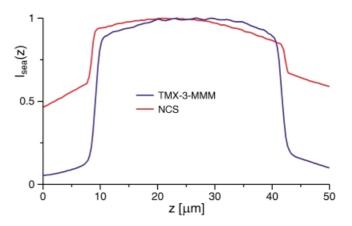

Fig. 5. Experimental fluorescence sea-response $I_{sea}(z)$ of the TMX-3-MMM and the NCS retrieved from a fluorescent immersion oil solution. Note the higher background of the NCS.

pinholes its sectioning ability would still be limited by a finite cross-talk. The same applies also to a non-TMX MMM, if its foci are adjusted to the same (small) interfocal distance. In this case, apart from the differences stemming from the used wavelengths, it will behave like a 'point-like pinhole' NCS.

As we were interested in concentrating on the performance of those systems that are realized in practice we also computed the sea-responses of the 50 μm diameter NCS and that of the TMX-3-MMM. Importantly, the calculation indicates that the decoupling the foci in three subgroups is sufficient in TMX-MMM to reduce the background under that of the NCS with point-like pinholes.

Experimental results

In this section we compare the axial sectioning of the TMX-3-MMM with the NCS. The implementation of TMX-3 in the MMM increases the distance between foci capable to interfere from the initial 5.6 μm to 8.8 μm. All experiments were carried out at the wavelength of $\lambda_{exc} = 488$ nm for the NCS and $\lambda_{exc} = 800$ nm for the MMM, as assumed in the theoretical part. The only exception were the experiments concerning the baker's yeast cells, *Saccharomyces cerevisiae*, which were carried out at the wavelength of $\lambda_{exc} = 890$ nm for the MMM.

The most severe test for the axial sectioning capability of a fluorescence microscope is the sea-response to a thick fluorescent layer. Figure 5 shows the sea-responses of a Rh6G-solution in immersion oil of ~30 μm thickness, as found with the NCS system with 50 μm diameter pinholes and the TMX-3-MMM. The profiles reveal that, whereas the NCS detects a substantial amount of fluorescence from out-of-focus-planes, the background of the TMX-3-MMM is almost negligible. For example, at a distance of 5 μm away from the focal point the background of the TMX-3-MMM is about seven times lower than that of the NCS. A hallmark of the NCS sea-response is that due to the background, the edge is found at much higher intensity levels.
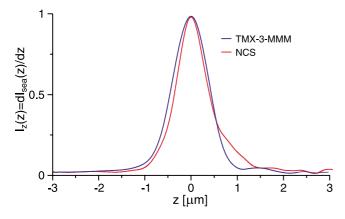
Fig. 6. Experimental fluorescence z-response $I_z(z)$ of the TMX-3-MMM and the NCS, derived from the sea-response.

The z-responses I_z of both microscopes is readily derived from the sea-response. The results are shown in Fig. 6. The curves feature an axial FWHM of 890 ± 20 nm for the MMM and a slightly smaller value of 790 ± 20 nm for the NCS. The reason for the slightly smaller value of the NCS is the shorter wavelengths involved in the single-photon excitaton mode. They are slightly broader than the theoretical values, which is probably due to aberrations.

In order to visualize the effects discussed herein in an application, we recorded 3D-stacks of 80 xy-images of an autofluorescent 25 µm diameter pollen grain featuring small spikes at its surface, and yeast. The pollen grains are excellent test objects for two reasons. First, they provide a strong autofluorescence signal. Second, they constitute very demanding test objects for 3D-imaging, because the bright spherical grain overwhelms the signal from the spikes above and beneath the grain. Hence, the ability of the microscope to discriminate the spikes is a stringent test for the axial sectioning capability of the system.

The results are shown in Fig. 7(a) and (b), comparing pollen grains of similar sizes taken with the NCS and the TMX-3-MMM. In each case, the combined surface/voltex plots of the 3D-data stack consist of 80 slices. The voltex representation visualizes the intensity of the pixels through a 'density-transparency feature' of the rendered 3D-object. Figure 7 reveals that there is a significant background in the case of the NCS, as anticipated from the curves in Figs 2–4 and in particular from that in Fig. 5. To render the comparison as fair as possible, the surface/voltex parameters were carefully selected. First, one has to realize that in order to visualize the surface of the pollen in each data set, different isosurface values are required. The reason is the difference in background for both systems. In analogy to the sea-response in Fig. 5, where the axial edge is found at much lower intensity levels in the TMX-3-MMM than in the NCS, the ideal surface reconstruction is achieved with an isosurface value of 8.2% of the maximum intensity for the MMM. In the NCS data, by contrast, because of the high background, the best value for representing the surface is 31.4%, which is about four times larger.

The voltex representation was tightly associated with the isosurface, so that the 100% value of the voltex is set to the individual isosurface values. In the case of the TMX-3-MMM, the voltex depicts the intensity distribution from the 3.9% to
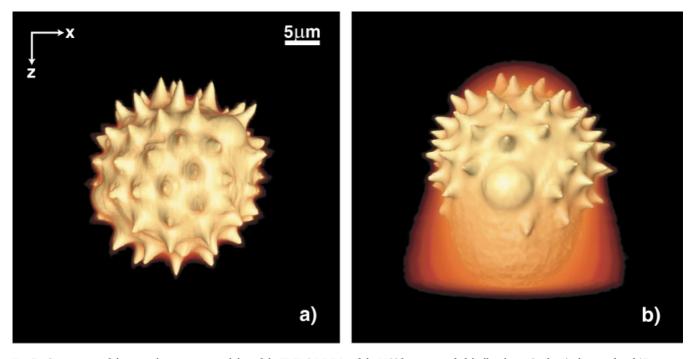

Fig. 7. Comparison of the optical sectioning capability of the TMX-3-MMM and the NCS for an extended, bulky object. Surface/voltex rendered 3D-image of two pollen grains of similar diameter (~25 µm). The TMX-3-MMM image (a) possesses a much lower background than its NCS counterpart (b).
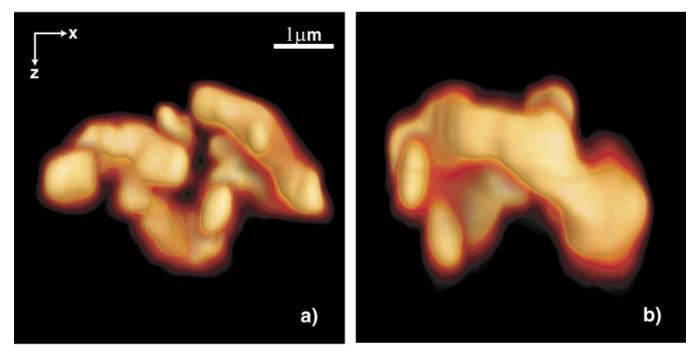
Fig. 8. Comparison of the optical sectioning capability of the TMX-3-MMM and the NCS for small objects. Surface/voltex plot of two *Saccharomyces cerevisiae* with GFP-labelled mitochondria (~6 μm). In the case of a small object, TMX-3-MMM (a) and NCS (b) show almost identical optical sectioning capabilities.

8.2% values of the maximum intensity of the data set. With respect to the isosurface value, the voltex representation ranges from 47.6% to 100%. The same percentage range was chosen for the NCS, which corresponds to the range 14.9–31.4% of the maximum intensity in the data. Contrasting the two 3D-data stacks reveals that the strong signal from the grain overcasts the signal of the spikes, which means that they cannot be axially discriminated. This applies particularly to the spikes beneath the pollen grain, i.e. to those that are deeper inside in the sample.

To pinpoint the optical sectioning capability of the two systems for non-extended objects, we also recorded 3D-stacks of baker's yeast cells, *S. cerevisiae*, with GFP-labelled mitochondria Fig. 8(a) and (b). The dimensions of these cells are in the order of a few micrometres. Moreover, the mitochondria are known to be of subresolution size, so that they do not constitute a 'bulky extended' object that is much larger than the wavelength, as is the case with the body of the pollen grain. Hence, no 'background' is anticipated. In Fig. 8(a) and (b) the isosurface and the voltex correspond to values of 20% and 5–20% of the maximum intensity, respectively. It is obvious from the data that in the case of a small object, MMM and NCS feature a comparable clarity of axial sectioning.

Discussion and conclusion

Whereas in MMM cross-talk can be eliminated by time-multiplexing, in parallelized single-photon excitation confocal microscopy it is a significant issue. The theoretical and experimental comparisons shown in this paper are useful for improving existing parallelized 3D-microscopes. First, the calculations in Figs 2 and 4 show that in the current NCS it would be advisable to have the option to decrease the pinhole diameter by a factor of 2. Whereas this would slightly reduce the visual perception of 'brightness' in the system, the critical cross-talk shoulder would be reduced by a factor of $\sqrt{3}$. However, although this is certainly technically possible, it might not be straightforward to implement. The requirement for detecting the fluorescence light through the same pinhole array is connected with stringent alignment conditions in the NCS. The illumination foci of the microlens disk must be perfectly matched onto the pinholes. The practical realization of this requirement is most likely challenged by the fact that the microlenses have to focus the light through an imaging-grade dichroic mirror (see Fig. 1a). The placement of this mirror between the microlens array and the pinhole disk is mandatory to achieve confocal sectioning. If the mirror is too thin (< 2 mm), it may not fulfil the flatness conditions required for aberration-free deflection of the fluorescence image onto the CCD-camera. For too large a thickness of the dichroic mirror, the illumination wavefronts will also be aberrated. Aberrations compromise the confocal effect and augment the cross-talk between the confocal channels.

The background-enhancing effect of aberrations is witnessed both in the responses of Figs 5 and 6, as well as in the NCS image of Fig. 7, where the spikes beneath the pollen grain

are not resolved. As these are the spikes that are further away from the cover slip, the aberrations are introduced by the grain itself or by the medium in which they are embedded. In this context, it is interesting to realize that the TMX-3-MMM counterpart images are clear, although in both systems the fluorescence generated in the pollen grain is imaged onto a CCD-camera. This indicates that the 'background' is not due to the back-imaging of the fluorescence. It is not the scattering of the fluorescence wavefronts by the grain that compromises the axial resolution in the NCS, it is rather the way in which the focal fields interact with each other in the particular system.

Aberrations are also the reason why the theoretical computations of Figs 2−4 can only reveal a tendency in the background signals, rather than a value perfectly matching an experiment (Egner & Hell, 2000). These aberrations may stem in part from the microlenses, but mostly from the sample and the mounting medium itself. Aberrations are critical because the overlap between the foci stems from the outer wings of the individual focal fields, where cross-talk is strongly enhanced.

Choosing the same voltex parameters for both data sets does not necessarily imply that the visual comparison of data in Fig. 7 is not deceptive, as one still can select the voltex parameters at will. We note that we have been seeking to select voltex parameters that would give best possible representation for the NCS data. After this selection the same parameters were applied to the TMX-3-MMM data.

Another remedy for reducing the cross-talk in the NCS would be the election of a larger distance between adjacent pinholes, for example, to the effective ∼6.8 µm of the TMX-3-MMM. This, however, would reduce the degree of parallelization per area by roughly an order of magnitude with respect to existing systems, so that it may not be desirable in fast imaging. The alternative strategy of allowing as much cross-talk as possible and subtracting it afterwards in form of a conventional image has been successfully pursued in the scanning aperture correlation microscope (Juškaitis et al., 1996). The cross-talk is of lesser importance when samples are very thin or sparse (Figs 8(a) and (b)), of course. In this case, high-quality 3D-reconstructions can be obtained even from a system that exhibits significant cross-talk. On the other hand, one has to realize that for comparatively thin specimens a sectioning microscope might not be required.

Clearly, the cross-talk depends on the ratio between the wavelength, interfocal distance, aperture, and for the NCS also on the pinhole size. The fact that the MMM requires a 1.5−2 times longer wavelength for the degree of parallelization per area is certainly a drawback of the MMM. The pinholes in the NCS have to be finite-sized in order to allow sufficient fluorescence to pass through and reach the detector. Due to the inherent sectioning property of non-linear excitation, there is no such requirement in the MMM. By overilluminating the back-aperture of the objective lens, one can ensure that the illumination foci approach dimensions that are close to the ideal values. On the other hand, extensive overillumination of the back-aperture is connected with significant losses of the pulsed (Ti:sapphire) laser light. This drawback of the MMM is slightly ameliorated by the fact that the laser light is coherent and therefore approaches faster the desired spatial confinement. In a sense, the need for a finite pinhole size augments cross-talk in the NCS; however, even if the pinholes were point-like, a parallelized confocal single-photon fluorescence microscope would not be able reach the performance of a single beam confocal fluorescence microscope, or of a TMX-N-MMM. Therefore, when comparing the pros and cons of the two systems for various design conditions, one should not lose sight of the fact that there is a straightforward all-optical solution to eliminate cross-talk of the excitation light in the MMM, but no obvious solution for NCS.

As the original parallelized Nipkow-disk scanning confocal microscope (Petran et al., 1968) used an 'incoherent' light source, such as an arc lamp, the question arises as to whether the latter would be useful in this context in NCS. With the appropriate excitation filters, the coherence length of a conventional light source is of the order of 20 µm; however, this is irrelevant. The destruction of the temporal coherence by TMX is ineffective in NCS, because the cross-talk of this approach stems from the finite transmittivity of the pinhole array. Even more serious will be the fact that the irradiance (power per area per steric angle) provided by a conventional light source will be insufficient to generate real-time images. The microlenses will not help, of course, as they cannot increase the irradiance of the light source. Hence for fluorescence imaging the NCS will have to use a laser or a similarly bright light source.

The results derived here for MMM can be extrapolated also to the related forms of parallelized non-linear microscopy, such as coherent anti-Stokes Raman scattering (CARS) and second and third harmonics generation. TMX applies perfectly well to these cases, but the coherence of the scattered non-linear signal leads to small differences to the fluorescence imaging case discussed herein. The advantage of the non-linear imaging modes is the near-infrared wavelength used, which enables deeper penetration into the specimen. Disadvantageous for the non-linear systems is the fact that the local intensity has to be carefully adjusted to a narrow range of typically $50-250 \, GW \, cm^{-2}$, so that it is high enough to generate a signal, but low enough to avoid photodamage. Intimately connected with this constraint is the fact that the non-linearly generated signal is usually lower than that produced by single-photon excitation.

In conclusion, the currently available NCS is a very useful system when fast and parallel imaging of comparatively thin or sparse objects is required. By reducing the pinhole diameter the system could probably be improved further. The TMX-MMM, by contrast, is superior in sectioning, which pays off in thicker and denser objects. The distinct advantage of the MMM over the NCS, however, is that its foci can be fully decoupled by time-multiplexing. Whereas even for point-like pinholes, parallelized single-photon microscopy faces the

parallelization limit, the pulsed non-linear systems can surmount it to achieve uncompromised axial sectioning.

Acknowledgements

References

Andresen, V., Egner, A. & Hell, S.W. (2001) Time-multiplexed multifocal multiphoton microscope. *Opt. Lett.* **26**, 75–77.

Bewersdorf, J., Pick, R. & Hell, S.W. (1998) Multifocal Multiphoton Microscopy. *Opt. Lett.* **23**, 655–657.

Buist, A.H., Müller, M., Squier, J. & Brakenhoff, G.J. (1998) Real time two-photon absorption microscopy using multipoint excitation. *J. Microsc.* **192**, 217–226.

Egner, A. & Hell, S.W. (2000) Time multiplexing and parallelization in multifocal multiphoton microscopy. *J. Opt. Soc. Am. A.* **17**, 1192–1201.

Fittinghoff, D.N., Wiseman, P.W. & Squier, J.A. (2000) Widefield multiphoton and temporally decorrelated multifocal multiphoton microscopy. *Opt. Express*, **7**, 273–279.

Ichihara, A., Tanaami, T., Isozaki, K., Sugiyama, Y., Kosugi, Y., Mikuriya, K., Abe, M. & Uemura, I. (1996) High-speed confocal fluorescence microscopy using a Nipkow scanner with microlenses for 3D-imaging of single fluorescent molecule in real time. *Bioimages*, **4**, 52–62.

Juškaitis, R., Wilson, T., Neil, M.A.A. & Kozubek, M. (1996) Efficient real-time confocal microscopy with white light sources. *Nature*, **383**, 804–806.

Kino, G.S. & Corle, T.R. (1989) Confocal scanning optical microscopy. *Phys. Today*, **42**, 55–62.

McCabe, E.M., Fewer, D.T., Ottewill, A.C., Hewlett, S.J. & Hegarty, J. (1996) Direct-view microscopy: optical sectioning strength for finite-sized, multiple-pinhole arrays. *J. Microsc.* **184**, 95–105.

Nielsen, T., Fricke, M., Hellweg, D. & Andresen, P. (2001) High efficiency beam splitter for multifocal multiphoton microscopy. *J. Microsc.* **201**, 368–376.

Petran, M., Hadravsky, M., Egger, M.D. & Galambos, R. (1968) Tandem-scanning reflected-light microscope. *J. Opt. Soc. Am.* **58**, 661–664.

Sheppard, C.J.R. & Wilson, T. (1981) The theory of the direct-view confocal microscope. *J. Microsc.* **124**, 107–117.

Straub, M., Lodemann, P., Holroyd, P., Jahn, R. & Hell, S.W. (2000) Live cell imaging by multifocal multiphoton microscopy. *Europ. J. Cell Biol.* **79**, 726–734.